

High-Temperature Low-Pressure Adsorption of Branched C₅–C₈ Alkanes on Zeolite Beta, ZSM-5, ZSM-22, Zeolite Y, and Mordenite

Joeri F. Denayer,[†] Wim Souverijns,[‡] Pierre A. Jacobs,[‡] Johan A. Martens,[‡] and Gino V. Baron^{*,†}

Department of Chemical Engineering, Vrije Universiteit Brussel, Pleinlaan 2, B-1050 Brussel, Belgium, and Center for Surface Chemistry and Catalysis, K.U. Leuven, Kardinaal Mercierlaan 92, B-3001 Heverlee, Belgium

Received: January 6, 1998; In Final Form: March 4, 1998

Henry constants, low-coverage adsorption enthalpies, van't Hoff preexponential factors, and separation factors of C₅–C₈ alkanes are determined on beta, ZSM-5, ZSM-22, mordenite, and Y zeolites at 473–648 K using tracer and perturbation chromatographic techniques. Three different adsorption behaviors were encountered depending on the zeolite type: (1) nonselective competitive adsorption of isoalkanes and *n*-alkanes inside the micropores (zeolite Y), (2) preferential adsorption of the *n*-alkanes over the isoalkanes inside the micropores (beta, ZSM-5 and mordenite), and (3) selective adsorption of the *n*-alkanes in the micropores and of the isoalkanes on the external crystal surfaces (ZSM-22). Linear and mono- and multibranched alkanes can be separated on columns of ZSM-22 and beta zeolites.

Introduction

Owing to the molecular dimensions of their micropore systems, zeolites possess the peculiar property of molecular shape selectivity, which is the possibility to discriminate among molecules based on differences in diffusivity, adsorptivity, or reactivity within the constrained environment of the zeolite microcavities.^{1,2} Molecular shape selectivity is at the basis of the successful applications of zeolites in catalytic and separation processes.³

An industrial separation process based on selective diffusion is the separation of linear and branched alkanes on zeolite 5A, applied in processes for boosting of the octane number of gasoline fractions and for the production of solvents, biodegradable detergents, and plasticizers.⁴ The zeolite 5A is however less suitable for separating isoalkanes according to their octane numbers.

Very few publications deal with separation of alkane isomers on molecular sieves other than zeolite 5A. Huddersman and Klimczyk^{5,6} reported the separation of 2,3-dimethylbutane and 2-methylpentane on mordenite and zeolite beta. The separation of octane, isooctane, and hexane with a silicalite-1 membrane was studied by Funke et al.⁷ Cavalcante and Ruthven^{8,9} determined adsorption equilibria and diffusional properties of branched C₆ isomers on silicalite-1 and suggested the separation of these isomers using selective diffusion and adsorption. From the chromatographic retention times of *n*-alkanes and isoalkanes on ZSM-22, ZSM-48, and silicalite-1 reported by Choudhary et al.,¹⁰ it can be deduced that the separation factors of these compounds on these zeolites should be large.

In the absence of steric constraints imposed by the adsorbent, isoalkanes and *n*-alkanes show a similar physisorption behavior.¹¹ Zeolites generally can discriminate among *n*- and isoalkanes and adsorb one group preferentially. Molecular sieves with 8-ring windows and pore sizes smaller than 5 Å

such as zeolite A adsorb preferentially the *n*-alkanes. Santilli et al.¹² reported the opposite behavior in 12-ring zeolites with tubular pores and pore diameters between 6.5 and 7.4 Å and found preferential adsorption of the branched hexanes over hexane. The phenomenon was most pronounced on SAPO-5. This zeolite property of selectively adsorbing the branched alkanes originates from the better matching of the molecular diameter of isoalkanes with the pore cross section and is referred to as *inverse shape selectivity*.¹²

Adsorption in the pore mouths at the crystal boundaries has to be invoked to rationalize the selective isomerization of long *n*-alkanes on the 10-ring bifunctional zeolite catalyst Pt/H-ZSM-22.¹³ According to the proposed model, long *n*-alkanes penetrate into a micropore of the zeolite crystal and undergo skeletal branching at positions in the micropore mouth. Multi-branching of alkanes has been proposed to involve key-lock adsorption of the alkanes, penetrating with their alkyl chains simultaneously into two or more adjacent pore openings.¹⁴

In a previous paper dealing with adsorption of *n*-alkanes on zeolites at 473–648 K,¹⁵ it was shown that the Henry adsorption constants K' obey a relationship with carbon number, CN:

$$K' = Ae^{BCN} \quad (1)$$

the A and B parameters depending strongly on the zeolite type and pore size. The exponential increase with carbon numbers can be explained by linear increases of adsorption enthalpies and entropies with carbon number.¹⁵ The strongest increase of the Henry constants with the carbon number (largest B parameters) occurs in 12-ring zeolites in which a moderate increase of the adsorption enthalpy is accompanied with a moderate loss of entropy. Although the adsorption enthalpy increases more rapidly with the carbon number, in 10-ring pores, the B parameters are lower owing to severe losses of degrees of freedom upon adsorption in these narrow pores. Obviously, zeolites exhibit a diversity of alkane adsorption behaviors.

[†] Vrije Universiteit Brussel.

[‡] K.U. Leuven.

TABLE 1: Adsorbent Properties

| | ZSM-5 | ZSM-22 | beta | mordenite | Na-Y | Na-USY |
|--|--------------------------------------|------------------|--------------------------------------|--------------------------------------|--------------------------------|------------|
| structure type ¹⁶ | MFI | TON | *BEA | MOR | FAU | FAU |
| oxygens in window | 10 | 10 | 12 | 12 | 12 | 12 |
| source, code | PQ, CBV 2802 | ref 17 | ref 18 | Zeocat | Zeocat | PQ, CBV760 |
| Si/Al | 137 | 30 | 12 | 5 | 2.7 | 30 |
| particle dimensions ^a (μm) | 0.4–0.8 | 1–4 \times 0.1 | 0.1–0.7 | 1.5 | 0.45 | n.a. |
| free-pore diameters ($\text{\AA} \times \text{\AA}$) | 5.4 \times 5.6 5.1 \times 5.5 | 4.5 \times 5.5 | 5.7 \times 7.5 5.6 \times 6.1 | 7.0 \times 6.5 2.6 \times 5.7 | supercage: 12.3 window: 7.3 | |

^a Determined by SEM.

TABLE 2: Column Properties and Experimental Conditions

| | ZSM-5 | ZSM-22 | beta | mordenite | Na-Y | Na-USY |
|--|-------|--------|-------------|-----------|------|--------|
| carrier gas | | | hydrogen | | | |
| temperature range | | | 473–648 K | | | |
| gas flow rates | | | 0.3–1 NmL/s | | | |
| L (m) | 0.20 | 0.27 | 0.10 | 0.15 | 0.25 | 0.26 |
| $\epsilon_{\text{macr}} + \epsilon_{\text{ext}}$ | 0.71 | 0.69 | 0.62 | 0.67 | 0.61 | 0.61 |

In this work, we have studied the adsorption and separation of C5–C8 alkane isomers on a representative series of 10- and 12-ring zeolites with different pore sizes and pore architectures (beta, ZSM-5, ZSM-22, Y, and mordenite) and at temperatures relevant to catalytic processes. It was investigated to what extent isoalkanes have access to the intracrystalline pore systems. Special attention was paid to ZSM-22, for which adsorption of isoalkanes on the external surfaces has been invoked to rationalize the catalytic performances.

Experimental Section

Adsorbents, Adsorbates, and Columns. The origin and further specifications of the zeolite samples are given in Table 1. As-synthesized ZSM-22 was calcined at 823 K, exchanged with ammonium chloride, and deammoniated at 673 K to obtain the H-form. The external surface of ZSM-22, determined by nitrogen adsorption and the t-plot method, was 80 m²/g. The number of pore mouths in ZSM-22 (estimated from the crystal size and morphology from SEM photographs) equals 330 \times 10^{−3} mol/g. The experiments were performed with the ZSM-5, ZSM-22, and mordenite samples in their H-form. With beta (synthesized according to ref 18) and USY, the catalytic transformations of the probe molecules were significant, and in those instances, Na-exchanged forms of these zeolite were used. To obtain the Na-form, beta and USY were contacted first with an aqueous solution of ammonium chloride and, subsequently, with a solution of sodium chloride.

The zeolite powders were compacted into disks by applying a pressure of ca. 20 MPa, and the disks were broken into fragments and sieved. The 400–500 μm fraction was filled into 1/8 in. diameter stainless steel columns with lengths of 0.10–0.30 m (shorter columns of 0.035 m were used for chromatographic separation experiments). Experimental conditions and column properties are given in Table 2.

Activation of the adsorbents was performed by raising the temperature at a rate of 1 K/min to 673 K and maintaining this temperature overnight. The gas flow rates were between 0.3 and 1 N mL/s. Pressure drop over the column varied between 0.05 and 0.1 bar. All alkanes used were of analytical grade and purchased from Acros.

Henry Constants. Henry constants K' were determined using the pulse chromatographic technique.¹⁹ In this technique, an inert gas carrier (hydrogen) is passed through a column filled with zeolite pellets. A mass flow controller (0–100 mL/min) regulates the flow rate of the hydrogen carrier gas. At the column inlet, a pulse (typically 0.1 μL) of a probe component

is injected. The pressure at the inlet of the column is monitored through a 10 bar pressure transducer. The column with adsorbent is placed in a Varian 3300 GC-oven. The outlet of the column is at atmospheric pressure. After passing the column, the gas stream enters the nonspecific thermal conductivity detector. After subtraction of the baseline from the response curve, first and second moments were calculated by integration. The dead time of the system (<1 s) was determined at different flow rates and subtracted from the experimental retention time. For nearly all measurements, this dead time was negligible compared to the retention time of the injected components. The retention time (first moment μ) of the response curve at the outlet of the column is related to the Henry constant as

$$\mu = \frac{L}{v_f} [(\epsilon_{\text{ext}} + \epsilon_{\text{macr}}) + (1 - \epsilon_{\text{ext}} - \epsilon_{\text{macr}})RT\rho_c K'] \quad (2)$$

in which L represents the column length, v_f the superficial gas velocity, ϵ_{ext} and ϵ_{macr} the external porosity and the porosity in macropores, R the gas constant, T the temperature, and ρ_c the crystal density, which was calculated assuming an ideal crystal structure.

The measurements were performed in the temperature range 473–648 K. Data points were taken at temperature intervals of 25 K. Replicate experiments resulted in variations of the first-order moment not larger than 1%. The coefficient of variation due to systematical errors on gas flow rates and column porosities of the Henry constants was calculated to be less than 5%.

To verify system linearity, the injection volume was changed over 1 order of magnitude. No variation of the retention time could be measured, indicating linear adsorption equilibrium. Since the Henry constants were independent of the gas flow rate, it could be concluded that the experiments were performed in equilibrium conditions and that no intrusion of mass transfer limitations occurred. van't Hoff plots of $\ln K'$ versus $1/T$ all had correlation factors R^2 larger than 0.999.

Adsorption Enthalpies. ΔH_0 (at zero coverage) were calculated from the temperature dependence of the Henry constants using the van't Hoff equation

$$K' = K'_0 e^{-\Delta H_0/RT} \quad (3)$$

The preexponential factor K'_0 of the van't Hoff equation is related to the entropy of adsorption $\Delta S_{0,\text{local}}^\ominus$ and the number of

TABLE 3: Henry Constants on Na-Y, Na-USY, Beta, Mordenite, ZSM-5, and ZSM-22 at 573 K, and at 548 K for Octane Isomers on Na-Y and Na-USY

| | K' (mol/(kg Pa)) | | | | | |
|---------------------|-----------------------|-----------------------|-----------------------|-----------------------|-----------------------|-----------------------|
| | Na-Y | Na-USY | beta | mordenite | ZSM-5 | ZSM-22 |
| <i>n</i> -pentane | 7.89×10^{-6} | 2.30×10^{-6} | 2.65×10^{-5} | 2.24×10^{-5} | 4.74×10^{-6} | 1.32×10^{-6} |
| 2-methylbutane | 7.93×10^{-6} | 2.16×10^{-6} | 1.48×10^{-5} | 1.42×10^{-5} | 3.34×10^{-6} | 3.23×10^{-7} |
| <i>n</i> -hexane | 1.86×10^{-5} | 4.12×10^{-6} | 8.03×10^{-5} | 7.71×10^{-5} | 9.73×10^{-6} | 2.59×10^{-6} |
| 2-methylpentane | 1.90×10^{-5} | 4.00×10^{-6} | 4.47×10^{-5} | 4.00×10^{-5} | 6.04×10^{-6} | 5.42×10^{-7} |
| 3-methylpentane | 1.95×10^{-5} | 4.34×10^{-6} | 3.66×10^{-5} | 2.81×10^{-5} | 5.23×10^{-6} | 4.42×10^{-7} |
| 2,2-dimethylbutane | 1.99×10^{-5} | 4.34×10^{-6} | 1.20×10^{-5} | 1.97×10^{-5} | 3.33×10^{-6} | 1.30×10^{-7} |
| 2,3-dimethylbutane | 1.96×10^{-5} | 4.38×10^{-6} | 2.39×10^{-5} | 2.21×10^{-5} | 3.12×10^{-6} | 2.39×10^{-7} |
| <i>n</i> -heptane | 4.20×10^{-5} | 7.80×10^{-6} | 2.54×10^{-4} | 2.66×10^{-4} | 1.96×10^{-5} | 4.66×10^{-6} |
| 2-methylhexane | 4.31×10^{-5} | 8.72×10^{-6} | 1.45×10^{-4} | 1.44×10^{-4} | 1.10×10^{-5} | 1.13×10^{-6} |
| 3-methylhexane | 4.43×10^{-5} | 7.91×10^{-6} | 1.01×10^{-4} | 7.34×10^{-5} | 1.04×10^{-5} | 8.71×10^{-7} |
| 2,3-dimethylpentane | 4.93×10^{-5} | 8.72×10^{-6} | 4.47×10^{-5} | 3.92×10^{-5} | 4.24×10^{-6} | 4.19×10^{-7} |
| 3,3-dimethylpentane | | | 3.12×10^{-5} | 3.12×10^{-5} | 6.95×10^{-6} | |

| | Na-Y | | Na-USY | | beta | mordenite | ZSM-5 | ZSM-22 |
|------------------------|-----------------------|-----------------------|-----------------------|-----------------------|-----------------------|-----------------------|-----------------------|-----------------------|
| | 548 K | 573 K | 548 K | 573 K | | | | |
| <i>n</i> -octane | 1.61×10^{-4} | 9.63×10^{-5} | 2.61×10^{-5} | 1.47×10^{-5} | 7.41×10^{-4} | 9.04×10^{-4} | 3.91×10^{-5} | 8.82×10^{-6} |
| 2-methylheptane | 1.67×10^{-4} | 9.88×10^{-5} | 2.49×10^{-5} | 1.45×10^{-5} | 4.19×10^{-4} | 4.78×10^{-4} | 2.15×10^{-5} | 2.04×10^{-6} |
| 3-methylheptane | 1.83×10^{-4} | 1.07×10^{-4} | | | 2.98×10^{-4} | 2.28×10^{-4} | 1.80×10^{-5} | 1.50×10^{-6} |
| 4-methylheptane | 1.77×10^{-4} | 1.05×10^{-4} | | | 2.55×10^{-4} | | 1.80×10^{-5} | 1.45×10^{-6} |
| 2,5-dimethylhexane | 1.92×10^{-4} | 1.10×10^{-4} | 2.65×10^{-5} | 1.51×10^{-5} | 2.33×10^{-4} | 2.28×10^{-4} | | 6.30×10^{-7} |
| 2,2,4-trimethylpentane | 2.09×10^{-4} | 1.24×10^{-4} | 2.94×10^{-5} | 1.81×10^{-5} | 4.02×10^{-5} | 6.93×10^{-5} | | 3.05×10^{-7} |

adsorption sites n_T as¹⁵

$$K_0' = \exp \left[\frac{\Delta S_{0,\text{local}}^\ominus}{R} + \ln \left(\frac{n_T}{2p^\ominus} \right) \right] \quad (4)$$

in which p^\ominus is the standard pressure, chosen as 0.1 MPa.

Adsorption isotherms were determined by perturbation chromatography.^{20,21} Before entering the chromatographic column, the hydrogen flow is passed through a reservoir filled with liquid hydrocarbon. The partial pressure of the hydrocarbon in the carrier flow can be adjusted by altering the temperature of the reservoir. The hydrogen/hydrocarbon equilibrium was calculated with the Redlich–Kwong–Soave model with Boston–Mathias modification. The mobile phase consisting of hydrogen and the probe hydrocarbon at a pressure p_i is perturbed by injecting a pulse of the probe component. The retention time of the perturbation is given by

$$\mu = \frac{L}{v_f} \left[(\epsilon_{\text{ext}} + \epsilon_{\text{macr}}) + (1 - \epsilon_{\text{ext}} - \epsilon_{\text{macr}})(1 - x) \frac{\partial q_i}{\partial p_i} \right] \quad (5)$$

The amount adsorbed q_i at a partial pressure p_i can be obtained by integration:

$$q_i(p) = \int_0^p \frac{\partial q_i}{\partial p_i} dp_i \quad (6)$$

Estimation of Lennard-Jones Adsorption Potentials with Computer Models. The adsorption potential of probe alkanes on ZSM-22 were estimated using an in-house-developed software package running on a personal computer with a Pentium 133 processor. A rigid fragment of a SiO₂ polymorph with ZSM-22 structure zeolite was generated using the crystallographic data from ref 22. The framework fragment was made large enough to avoid boundary effects (1920 oxygen atoms). Geometry optimization of the hydrocarbon molecules was performed via HYPERChem V 3.0 for Windows. The molecules were optimized in an MM⁺ force field in a vacuum until a RMS gradient (total energy gradient calculated as a root-mean-square gradient) of 4×10^{-5} kJ mol⁻¹ was reached. Success-

sively, a steepest descent, Fletcher–Reeves and Newton–Raphson optimization algorithm was applied to reach the final optimized molecule.

The adsorption potential $U_{L-J}(r_{ij})$ was calculated using a 12/6 Lennard-Jones potential function summed over all atoms:

$$U_{L-J}(r_{ij}) = \sum_{ij} \left(\frac{A_{ij}}{(r_{ij})^{12}} - \frac{B_{ij}}{(r_{ij})^6} \right) \quad (7)$$

with r_{ij} denoting the distance between two interacting atomic (or molecular) centers and A_{ij} and B_{ij} the repulsive and dispersive interaction parameters, respectively. Values for A_{ij} and B_{ij} for oxygen–hydrogen and oxygen–carbon interactions valid for silicon dioxide frameworks were obtained from ref 23. For the position optimization of hydrocarbons on the external [100] and [010] crystal faces and the micropores the hydrocarbon was docked manually into the framework fragment. Then, the position with lowest potential was searched via a three-dimensional rotation–translation procedure using a steepest descent algorithm. To avoid local minima, the translation and rotation step size were increased again whenever the hydrocarbon had reached an optimum.

Results

The zeolites selected for this study are representative for the different types of pore structures:¹⁶ zeolite Y has a three-dimensional pore network, consisting of large spherical cavities (free diameter of ca. 12 Å), interconnected through windows with a diameter of ca. 7.3 Å. Zeolite beta has an intersecting tube type of pore structure, with free diameters in the tube segments of 5.6–7.5 Å. Mordenite is essentially a monodimensional tubular pore system, with pore cross sections of 7.0×6.5 Å. ZSM-5 has an intersecting tube type of micropore system with free diameters in the tubes of 5.1–5.6 Å. ZSM-22 has a unidimensional tubular pore system with a small pore cross section of 4.5×5.5 Å.

Henry Constants of Alkanes. The Henry constants of iso- and *n*-alkanes at 573 K on the different zeolites are listed in Table 3 and plotted against carbon number in Figure 1. On Na-Y and Na-USY, the Henry constants increase with increasing

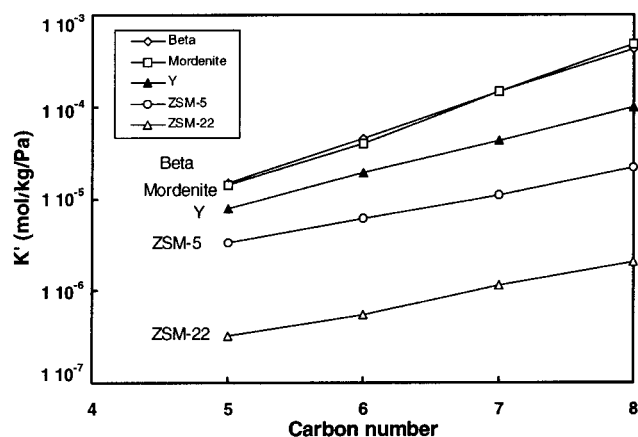


Figure 2. Henry constants of 2-methyl-branched alkanes with different carbon number on Na-Y, beta, mordenite, ZSM-5, and ZSM-22 at 573 K.

(Figure 1, Table 3). The more the carbon skeleton is branched, the lower the Henry constants:

$$K'(n\text{-alkane}) > K'(\text{monomethyl-branched isoalkane}) > K'(\text{dimethyl-branched isoalkane}) > K'(\text{trimethyl-branched isoalkane}) \quad (8)$$

On beta, mordenite, and ZSM-22, the Henry constants also decrease when the methyl side chain moves toward the center of the alkane chain:

$$K'(2\text{-MeC7}) > K'(3\text{-MeC7}) > K'(4\text{-MeC7}) \quad (9)$$

On ZSM-5, no difference in Henry constant between 3- and 4-MeC7 was observed.

TABLE 5: Coefficients A and B of the Correlation $K' = Ae^{BCN}$ between Henry Constants and Carbon Number for the Linear and 2-Methyl-Branched Alkanes at 573 K (Standard Errors Are Indicated)

| | A | | B | |
|-----------|----------------------------------|----------------------------------|-------------------|-------------------|
| | linear | 2-Me branched | linear | 2-Me branched |
| Na-Y | $(1.29 \pm 0.05) \times 10^{-7}$ | $(1.21 \pm 0.09) \times 10^{-7}$ | 0.827 ± 0.006 | 0.839 ± 0.010 |
| Na-USY | $(9.01 \pm 0.63) \times 10^{-8}$ | $(8.91 \pm 0.40) \times 10^{-8}$ | 0.640 ± 0.009 | 0.636 ± 0.007 |
| beta | $(1.02 \pm 0.04) \times 10^{-7}$ | $(5.46 \pm 0.19) \times 10^{-8}$ | 1.11 ± 0.04 | 1.12 ± 0.04 |
| mordenite | $(4.71 \pm 0.07) \times 10^{-8}$ | $(3.62 \pm 0.07) \times 10^{-8}$ | 1.23 ± 0.02 | 1.18 ± 0.03 |
| ZSM-5 | $(1.43 \pm 0.01) \times 10^{-7}$ | $(1.49 \pm 0.01) \times 10^{-7}$ | 0.702 ± 0.005 | 0.620 ± 0.010 |
| ZSM-22 | $(5.79 \pm 0.44) \times 10^{-8}$ | $(1.36 \pm 0.36) \times 10^{-8}$ | 0.629 ± 0.011 | 0.626 ± 0.036 |

TABLE 6: Adsorption Enthalpy at Zero Coverage on Na-Y, Na-USY, Beta, Mordenite, ZSM-5, ZSM-22, and Methylsilicone (Standard Errors Indicated)

| | $-\Delta H_0$ (kJ/mol) | | | | | | |
|------------------------|------------------------|-----------------|-----------------|-----------------|-----------------|-----------------|-----------------------------|
| | Na-Y | Na-USY | beta | mordenite | ZSM-5 | ZSM-22 | methylsilicone ^a |
| <i>n</i> -pentane | 39.4 ± 0.35 | 40.4 ± 0.42 | 53.0 ± 0.49 | 55.7 ± 0.64 | 57.7 ± 0.42 | 62.1 ± 2.00 | |
| 2-methylbutane | 39.2 ± 0.24 | 40.0 ± 0.41 | 51.0 ± 0.52 | 55.6 ± 0.67 | 56.1 ± 1.4 | 50.4 ± 1.4 | |
| <i>n</i> -hexane | 45.5 ± 0.32 | 47.7 ± 0.35 | 62.7 ± 0.46 | 67.1 ± 0.80 | 68.8 ± 0.26 | 75.0 ± 1.3 | 28.4 ± 0.3 |
| 2-methylpentane | 45.3 ± 0.23 | 46.6 ± 0.54 | 60.8 ± 0.51 | 65.8 ± 0.82 | 66.8 ± 0.22 | 62.4 ± 1.2 | 27.2 |
| 3-methylpentane | 44.5 ± 0.42 | 46.3 ± 0.25 | 60.0 ± 0.49 | 64.5 ± 0.82 | 66.0 ± 0.18 | 61.7 ± 2.1 | 27.5 |
| 2,2-dimethylbutane | 43.2 ± 0.38 | 45.4 ± 0.46 | 54.1 ± 0.41 | 62.9 ± 0.49 | 63.9 ± 1.22 | 38.2 ± 3.1 | 25.4 |
| 2,3-dimethylbutane | 44.1 ± 0.28 | 46.1 ± 0.53 | 59.5 ± 0.41 | 63.4 ± 0.72 | 63.4 ± 1.49 | 52.2 ± 2.9 | 26.5 |
| <i>n</i> -heptane | 51.9 ± 0.39 | 54.0 ± 0.44 | 72.6 ± 0.78 | 77.0 ± 1.16 | 79.6 ± 0.26 | 87.9 ± 0.7 | 32.3 |
| 2-methylhexane | 51.6 ± 0.31 | | 70.4 ± 0.25 | 75.1 ± 1.41 | 78.4 ± 0.44 | 75.4 ± 1.3 | |
| 3-methylhexane | 51.4 ± 0.23 | 53.5 ± 0.33 | 69.7 ± 0.39 | 75.4 ± 1.24 | 78.0 ± 1.25 | 69.8 ± 2.4 | 31.1 |
| 2,3-dimethylpentane | 50.6 ± 0.21 | 52.0 ± 0.27 | 67.7 ± 0.53 | 74.7 ± 1.08 | 74.1 ± 0.96 | 60.2 ± 2.9 | 30.1 |
| <i>n</i> -octane | 57.5 ± 0.23 | 60.1 ± 0.24 | 82.9 ± 0.55 | 87.3 ± 1.48 | 90.7 ± 0.28 | 100.5 ± 0.8 | 36.3 |
| 2-methylheptane | 57.2 ± 0.36 | 59.0 ± 0.30 | 81.2 ± 0.73 | 85.1 ± 0.61 | 88.6 ± 0.34 | 84.5 ± 1.6 | 34.7 |
| 3-methylheptane | 57.3 ± 0.30 | 57.3 ± 0.27 | 80.9 ± 0.62 | 83.1 ± 1.05 | 88.5 ± 0.37 | 74.4 ± 1.7 | |
| 4-methylheptane | 57.2 ± 0.40 | 57.2 ± 0.29 | 81.1 ± 0.41 | 81.8 ± 1.37 | 88.7 ± 0.45 | 77.7 ± 1.8 | |
| 2,5-dimethylhexane | 57.1 ± 0.28 | 57.6 ± 0.42 | | | | 60.2 ± 1.9 | 33.1 |
| 2,2,4-trimethylpentane | 56.8 ± 0.22 | 57.5 ± 0.28 | 73.4 ± 0.54 | 76.8 ± 1.32 | | 48.2 ± 3.1 | 31.2 |

^a Nonpolar reference material, data retrieved from the work of Castello and d'Amato (1975).¹¹

On ZSM-22, the Henry constants of isoalkanes are more than 1 order of magnitude smaller than on the other zeolites (Table 3).

Henry constants of the 2-methyl-monobranched alkanes at 573 K are plotted against carbon number in Figure 2. An exponential increase of the Henry constant with carbon number previously observed with *n*-alkanes (see eq 1) is now observed with 2-methyl-branched alkanes. The coefficients A and B for 2-methyl-branched alkanes and linear alkanes according to eq 1 are listed in Table 5.

Adsorption Enthalpies. The adsorption enthalpies at zero coverage of the linear and branched alkanes on Na-Y, Na-USY, beta, mordenite, ZSM-22, ZSM-5, and methylsilicone as reference are given in Table 6. On Na-Y, Na-USY, beta, mordenite, and ZSM-5, the adsorption enthalpies of branched alkanes are not more than 10 kJ/mol lower than for the corresponding linear alkanes, the difference becoming larger with increasing degree of branching. On ZSM-22, much larger differences are observed, amounting to even more than 50 kJ/mol for octane and 2,2,4-trimethylpentane (Table 6). A linear relationship between the enthalpy of adsorption of linear and 2-methyl-branched alkanes and the carbon number has been fitted to the experimental data (Table 7):

$$-\Delta H_0 = \alpha CN + \beta \quad (10)$$

On Na-Y, Na-USY, beta, and ZSM-5, the α values for linear and 2-methyl-branched isomers are almost identical, while on ZSM-22 and mordenite, the adsorption enthalpies of 2-methyl-branched alkanes increase with about 1 kJ/mol less per added carbon atom compared to the linear alkanes (Table 7).

The Lennard-Jones adsorption potentials calculated for hexane and its isomers inside the micropores and on external crystal

TABLE 7: Relationships between Adsorption Enthalpies, Preexponential Factors, and the Carbon Number of Linear and 2-Methyl-Branched Alkanes on Na-Y, Na-USY, Beta, Mordenite, ZSM-5, and ZSM-22

| | $-\Delta H_0$ (kJ/mol) | | $-\ln(K_0)$ | |
|-----------|---------------------------------|---------------------------------|----------------------------------|----------------------------------|
| | linear | 2-Me branched | linear | 2-Me branched |
| Na-Y | (6.07 ± 0.10)CN + (9.12 ± 0.94) | (6.03 ± 0.04)CN + (9.13 ± 0.23) | (0.541 ± 0.020)CN + (16.7 ± 0.1) | (0.502 ± 0.008)CN + (16.8 ± 0.1) |
| Na-USY | (6.51 ± 0.06)CN + (8.21 ± 0.50) | (6.31 ± 0.10)CN + (8.56 ± 0.64) | (0.757 ± 0.034)CN + (17.4 ± 0.2) | (0.748 ± 0.008)CN + (17.4 ± 0.1) |
| beta | (10.0 ± 0.1)CN + (2.58 ± 0.61) | (10.0 ± 0.20)CN + (0.8 ± 1.33) | (0.973 ± 0.008)CN + (16.8 ± 0.1) | (1.02 ± 0.04)CN + (16.6 ± 0.2) |
| mordenite | (10.5 ± 0.2)CN + (3.50 ± 1.45) | (9.77 ± 0.12)CN + (6.87 ± 0.78) | (1.03 ± 0.05)CN + (17.2 ± 0.4) | (1.00 ± 0.03)CN + (17.63 ± 0.2) |
| ZSM-5 | (11.0 ± 0.1)CN + (2.8 ± 0.93) | (10.9 ± 0.05)CN + (1.56 ± 0.32) | (1.60 ± 0.01)CN + (16.4 ± 0.1) | (1.67 ± 0.01)CN + (16.0 ± 0.0) |
| ZSM-22 | (12.2 ± 0.2)CN + (1.7 ± 1.56) | (11.5 ± 0.23)CN - (6.77 ± 1.51) | (1.91 ± 0.05)CN + (16.9 ± 0.4) | (2.09 ± 0.09)CN + (15.0 ± 0.6) |

TABLE 8: Calculated Lennard-Jones Potentials for C₆ Isomers on External Faces and in the Micropores of ZSM-22 Fragment

| | $-\Delta H_0$ (kJ/mol) | | | |
|--------------------|------------------------|------------|------------|------------------------------|
| | inside micropore | [100] face | [010] face | average [100] and [010] face |
| hexane | 90.5 | 54.4 | 55.6 | 55.0 |
| 2-methylpentane | 99.0 | 53.3 | 55.6 | 54.5 |
| 3-methylpentane | 91.7 | 47.4 | 53 | 50.2 |
| 2,2-dimethylbutane | 27.5 | 44.4 | 43 | 43.5 |
| 2,3-dimethylbutane | 85.7 | 51.8 | 50.3 | 51.1 |

faces of ZSM-22 are given in Table 8. ZSM-22 crystals have a needle type of morphology. The micropores run in the [001] crystallographic direction. The external surfaces were modeled by terminating the framework fragment with [010] and [100] planes through the midpoints of the 10-ring windows. On the external surfaces, the Lennard-Jones adsorption potentials for the isohexanes are all around 50 kJ mol⁻¹ (Table 8). In the micropores, the differences between the isomers are much more pronounced. 2,2-Dimethylbutane has a low adsorption potential, amounting 27.5 kJ mol⁻¹. 2-Methylpentane has a larger adsorption potential (99 kJ mol⁻¹) than *n*-hexane (90.5 kJ mol⁻¹), but encounters very large energy barriers between the optimal positions in the channel. 3-Methylpentane and 2,3-dimethylbutane also have much larger adsorption potentials in the pores than on the external surface.

Preexponential Factors. The preexponential factors, K_0' of the van't Hoff equation are reported in Table 9. In Na-Y and Na-USY, the K_0' values are little influenced by branching of the carbon skeletons. On ZSM-22, the K_0' values of branched alkanes are significantly larger than for *n*-alkanes, while on ZSM-5, beta, and mordenite, K_0' values of branched alkanes are systematically somewhat smaller than for *n*-alkanes.

The evolution of the preexponential factors with the carbon number of linear and 2-methyl-branched can be fitted with linear relationships:

$$-\ln K_0' = \gamma \text{CN} + \delta \quad (11)$$

for which the γ and δ parameters are given in Table 7.

Adsorption isotherms at 506 K of heptane, 2-methylhexane, and 2,3-dimethylpentane on ZSM-22 are shown in Figure 3. The saturation capacities of heptane, 2-methylhexane, and 2,3-dimethylbutane are ca. 0.2, 0.04, and 0.008 mol/kg, respectively.

The separation of a mixture of hexane isomers and octane isomers on a column of zeolite beta is shown in Figure 4. In this type of experiment, a mixture containing typically 0.2 μ L of each component was injected in the column. A good separation of *n*-hexane, the hexane isomers with one methyl side chain, and 2,2-dimethylbutane is obtained, and this with a column containing only about 10 theoretical plates. It was also possible to separate *n*-octane, 2-methylheptane, and 2,2,4-trimethylpentane.

The separation of pentane, hexane, heptane, and octane isomers on a ZSM-22 column (with about 100 theoretical plates) is shown in Figure 5. The different alkanes are reasonably well separated from each other. ZSM-22 has the ability to separate pentane, hexane, heptane, and octane isomers individually.

Discussion

Na-Y Zeolite. The alkane molecules studied can be easily accommodated in the supercages of these faujasite type zeolites. In a previous study on *n*-alkane adsorption on Y zeolites,¹⁵ it was shown that at low surface coverage, adsorption occurs preferentially on the Brønsted acid sites and on the alkali metal cations of the zeolite. Compared to *n*-alkanes, isoalkanes are now found to have slightly lower adsorption enthalpies (Table 6) and larger preexponential factors (Table 8). Assuming that the number of adsorption sites for *n*- and isoalkanes with the same carbon number is the same, larger preexponential factors reflect smaller adsorption entropies (eq 4). Owing to their ramified skeletons, the isoalkanes are weaker adsorbed, lose less degrees of freedom upon adsorption, and jump more frequently from site to site.

The preexponential factors of isoalkanes increase less with the carbon number than for *n*-alkanes (Table 7). This is another manifestation of the differences in mobility being less pronounced with isoalkanes than with *n*-alkanes.

For a given carbon number, the Henry constants increase with increasing degree of branching (Table 3 and Table 4), indicating that skeletal branching of the adsorbate has a stronger influence on the preexponential factor than on the enthalpy term of the van't Hoff equation (eq 3).

Na-USY Zeolite. Isolation of the adsorption sites for *n*-alkanes in Y zeolites by dealumination leads to more difficult jumps from site to site.¹⁵ In the present study with branched alkanes, it is found that the preexponential factors in Na-USY are less sensitive to the degree of branching of the adsorbate than in Na-Y (Table 9). Consequently, in Na-USY, the mobility of iso- compared to *n*-alkanes is more similar, in agreement with the site-to-site jump model. This explains why the differences in Henry constants between linear and branched alkanes is smaller on Na-USY than on Na-Y (Table 4).

ZSM-22. Among the zeolites investigated, ZSM-22 exhibits the highest adsorption enthalpies for *n*-alkanes (Table 6), reflecting the strong interaction of the *n*-alkanes with the narrow tubular micropores of this zeolite.²⁴ This strong interaction is also reflected in the large increments of the adsorption enthalpy with carbon numbers (Table 7). The adsorption enthalpies of monomethyl-branched alkanes on ZSM-22 are systematically lower than on ZSM-5, and those for dimethyl-branched and trimethyl-branched alkanes are in the range of values found with Y type zeolites (Table 6). On ZSM-22, the adsorption enthalpies change dramatically with the degree of branching. For comparison, on dimethylsilicone, a nonpolar and nonporous adsorbent, branching of the carbon skeleton results in a much smaller decrease of the adsorption enthalpy (Table 6). Lennard-Jones

TABLE 9: Preexponential Factors of the van't Hoff Equation of Linear and Branched Alkanes on Na-Y, Na-USY, Beta, Mordenite, ZSM-5, and ZSM-22 (Standard Errors Indicated)

| | K_0' (mol/kg/Pa) | | | | | |
|------------------------|-----------------------------------|-----------------------------------|-----------------------------------|-----------------------------------|-----------------------------------|-----------------------------------|
| | Na-Y | Na-USY | beta | mordenite | ZSM-5 | ZSM-22 |
| <i>n</i> -pentane | $(3.90 \pm 0.27) \times 10^{-9}$ | $(6.19 \pm 0.12) \times 10^{-10}$ | $(3.88 \pm 0.17) \times 10^{-10}$ | $(1.83 \pm 0.17) \times 10^{-10}$ | $(2.59 \pm 0.35) \times 10^{-11}$ | $(3.10 \pm 0.89) \times 10^{-12}$ |
| 2-methylbutane | $(4.02 \pm 0.29) \times 10^{-9}$ | $(6.36 \pm 0.14) \times 10^{-10}$ | $(3.78 \pm 0.18) \times 10^{-10}$ | $(1.49 \pm 0.59) \times 10^{-10}$ | $(2.56 \pm 0.29) \times 10^{-11}$ | $(8.51 \pm 3.71) \times 10^{-12}$ |
| <i>n</i> -hexane | $(2.20 \pm 0.21) \times 10^{-9}$ | $(2.88 \pm 0.15) \times 10^{-10}$ | $(1.54 \pm 0.06) \times 10^{-10}$ | $(8.00 \pm 0.22) \times 10^{-11}$ | $(5.17 \pm 0.31) \times 10^{-12}$ | $(4.59 \pm 1.10) \times 10^{-13}$ |
| 2-methylpentane | $(2.37 \pm 0.26) \times 10^{-9}$ | $(3.08 \pm 0.19) \times 10^{-10}$ | $(1.25 \pm 0.06) \times 10^{-10}$ | $(5.50 \pm 0.16) \times 10^{-11}$ | $(4.88 \pm 0.19) \times 10^{-12}$ | $(1.40 \pm 0.31) \times 10^{-12}$ |
| 3-methylpentane | $(2.88 \pm 0.33) \times 10^{-9}$ | $(3.43 \pm 0.15) \times 10^{-10}$ | $(1.21 \pm 0.05) \times 10^{-10}$ | $(5.01 \pm 0.11) \times 10^{-11}$ | $(5.00 \pm 0.55) \times 10^{-12}$ | $(1.20 \pm 0.48) \times 10^{-12}$ |
| 2,2-dimethylbutane | $(3.72 \pm 0.62) \times 10^{-9}$ | $(4.11 \pm 0.35) \times 10^{-10}$ | $(1.41 \pm 0.05) \times 10^{-10}$ | $(4.94 \pm 0.09) \times 10^{-11}$ | $(4.94 \pm 0.46) \times 10^{-12}$ | $(4.58 \pm 1.45) \times 10^{-11}$ |
| 2,3-dimethylbutane | $(3.21 \pm 0.49) \times 10^{-9}$ | $(3.59 \pm 0.27) \times 10^{-10}$ | $(8.86 \pm 0.3) \times 10^{-11}$ | $(4.88 \pm 0.13) \times 10^{-11}$ | $(5.15 \pm 0.29) \times 10^{-12}$ | $(6.61 \pm 3.12) \times 10^{-12}$ |
| <i>n</i> -heptane | $(1.40 \pm 0.13) \times 10^{-9}$ | $(1.50 \pm 0.14) \times 10^{-10}$ | $(5.84 \pm 0.5) \times 10^{-11}$ | $(2.30 \pm 0.12) \times 10^{-11}$ | $(1.08 \pm 0.07) \times 10^{-12}$ | $(6.27 \pm 1.27) \times 10^{-14}$ |
| 2-methylhexane | $(1.50 \pm 0.11) \times 10^{-9}$ | | $(5.24 \pm 0.14) \times 10^{-11}$ | $(1.81 \pm 0.17) \times 10^{-11}$ | $(7.78 \pm 0.78) \times 10^{-13}$ | $(1.27 \pm 1.04) \times 10^{-13}$ |
| 3-methylhexane | $(1.61 \pm 0.13) \times 10^{-9}$ | $(1.80 \pm 0.14) \times 10^{-10}$ | $(4.34 \pm 0.19) \times 10^{-11}$ | $(8.68 \pm 0.59) \times 10^{-12}$ | $(8.03 \pm 0.92) \times 10^{-13}$ | $(2.81 \pm 1.15) \times 10^{-13}$ |
| 2,3-dimethylpentane | $(2.15 \pm 0.16) \times 10^{-9}$ | $(2.22 \pm 0.13) \times 10^{-10}$ | $(3.07 \pm 0.18) \times 10^{-11}$ | $(5.38 \pm 0.31) \times 10^{-12}$ | $(7.41 \pm 0.19) \times 10^{-13}$ | $(8.59 \pm 1.17) \times 10^{-12}$ |
| <i>n</i> -octane | $(7.47 \pm 0.78) \times 10^{-10}$ | $(6.16 \pm 0.34) \times 10^{-11}$ | $(2.09 \pm 0.22) \times 10^{-11}$ | $(9.00 \pm 1.01) \times 10^{-12}$ | $(2.09 \pm 0.14) \times 10^{-13}$ | $(1.04 \pm 0.41) \times 10^{-14}$ |
| 2-methylheptane | $(8.79 \pm 0.45) \times 10^{-10}$ | $(6.78 \pm 0.21) \times 10^{-11}$ | $(1.67 \pm 0.24) \times 10^{-11}$ | $(7.66 \pm 0.93) \times 10^{-12}$ | $(1.79 \pm 0.14) \times 10^{-13}$ | $(1.81 \pm 1.41) \times 10^{-14}$ |
| 3-methylheptane | $(9.04 \pm 0.35) \times 10^{-10}$ | | $(1.23 \pm 0.19) \times 10^{-11}$ | $(5.37 \pm 0.10) \times 10^{-12}$ | $(1.70 \pm 0.13) \times 10^{-13}$ | $(6.23 \pm 1.28) \times 10^{-14}$ |
| 4-methylheptane | $(8.99 \pm 0.56) \times 10^{-10}$ | | $(1.03 \pm 0.21) \times 10^{-11}$ | $(4.64 \pm 0.08) \times 10^{-12}$ | $(1.63 \pm 0.17) \times 10^{-13}$ | $(5.28 \pm 0.92) \times 10^{-14}$ |
| 2,5-dimethylhexane | $(9.10 \pm 0.94) \times 10^{-10}$ | $(7.21 \pm 0.10) \times 10^{-11}$ | | | | $(8.38 \pm 5.97) \times 10^{-13}$ |
| 2,2,4-trimethylpentane | $(1.21 \pm 0.13) \times 10^{-9}$ | $(8.94 \pm 0.29) \times 10^{-11}$ | $(8.34 \pm 1.82) \times 10^{-12}$ | $(6.13 \pm 0.07) \times 10^{-12}$ | | $(2.86 \pm 0.74) \times 10^{-12}$ |

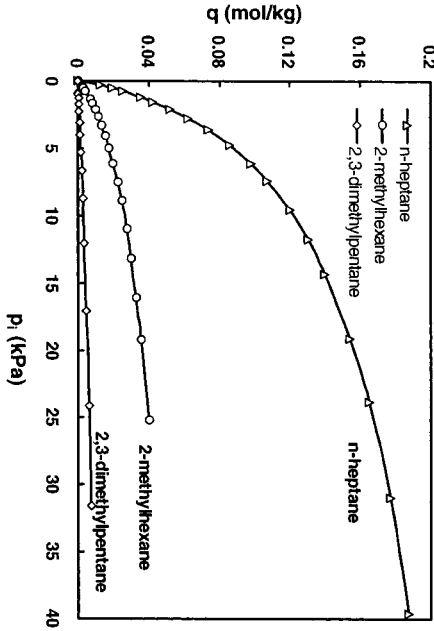


Figure 3. Adsorption isotherms of *n*-heptane, 2-methylhexane, 2-methylpentane, and 2,3-dimethylpentane on ZSM-22 at 506 K.

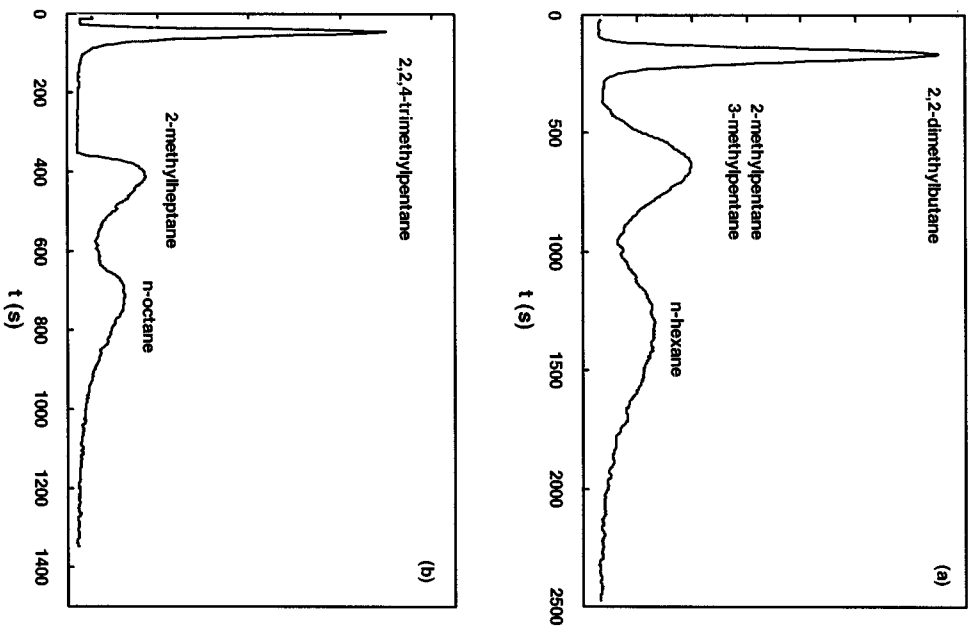


Figure 4. Chromatographic separation of linear and branched alkanes on zeolite beta: (a) *n*-hexane, 2-methylpentane, 3-methylpentane, and 2,2-dimethylbutane at 473 K; (b) *n*-octane, 2-methylheptane, and 2,2,4-trimethylpentane at 573 K.

potential energies calculated on the external crystal surfaces and in the pores of ZSM-22 (Table 8) indicate that adsorption on external crystal faces cannot account for this effect. In the pores, the calculated adsorption potentials of 2- and 3-methylpentane are larger than that of *n*-hexane, whereas the opposite was observed experimentally. For 2,2-dimethylbutane, the repulsion forces dominate the adsorption potential, which is very low in the pores. The experimentally observed differences between

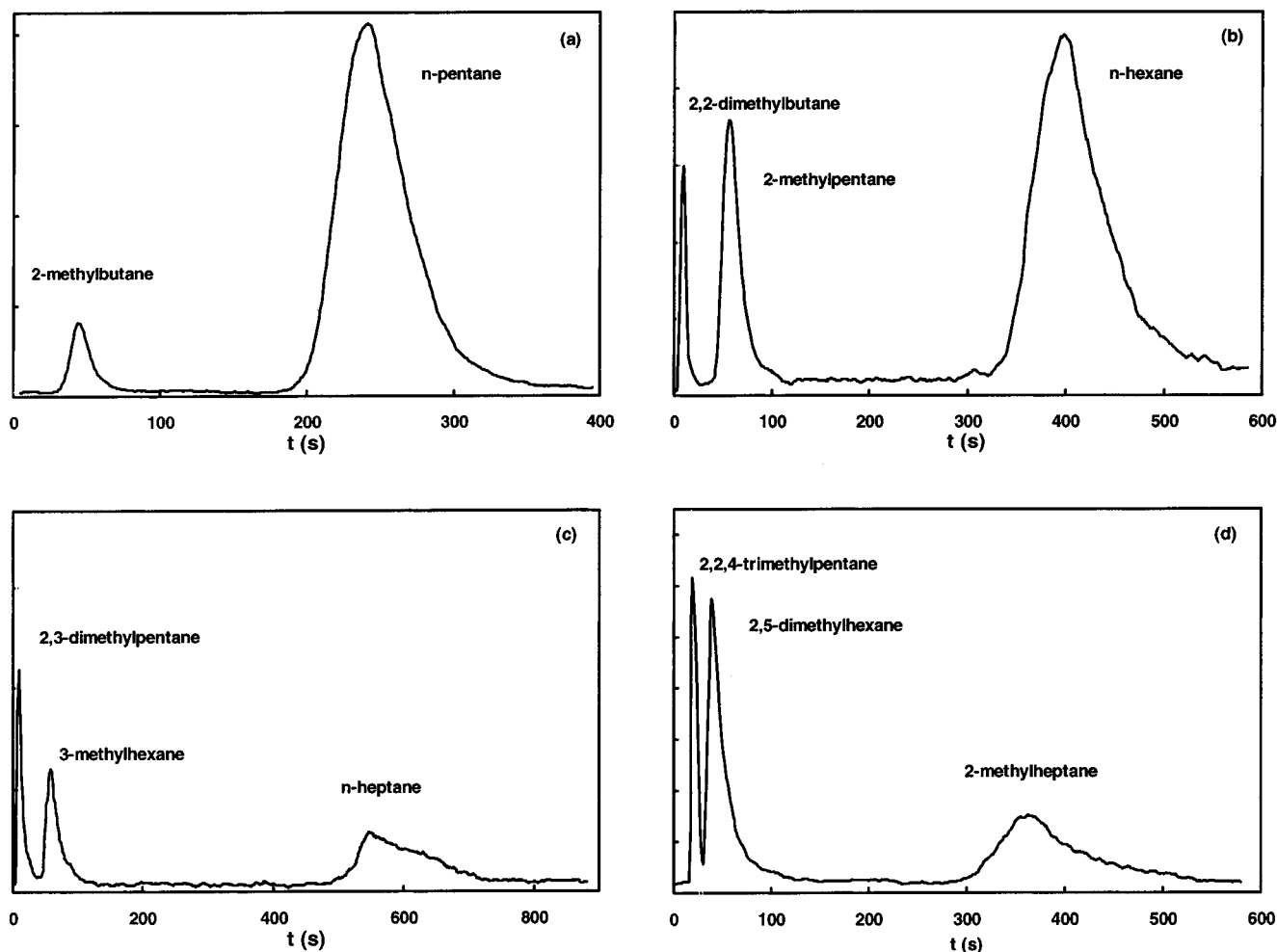


Figure 5. Chromatographic separation of linear and branched alkanes on zeolite ZSM-22 at 473 K: (a) *n*-pentane and 2-methylbutane; (b) *n*-hexane, 2-methylpentane and 2,2-dimethylbutane; (c) *n*-heptane, 3-methylhexane, and 2,3-dimethylpentane; (d) 2-methylheptane, 2,5-dimethylhexane, and 2,2,4-trimethylpentane.

n- and isoalkanes cannot be explained by adsorption in the pores, nor by adsorption on the external surface.

The fast increase of the adsorption enthalpy of the 2-methyl-branched isomers with the carbon number (11 kJ/mol per CH₂ added, Table 7) also indicates that at least a part of the branched molecules interacts with the intracrystalline force field.

On ZSM-22, the preexponential factors of the van't Hoff equation for isoalkanes are up to 2 orders of magnitude larger than those for the *n*-alkanes (Table 9). According to eq 4, this difference originates either from a higher number of adsorption sites or from a lower adsorption entropy. Owing to the bulkiness of the isoalkanes, the number of accessible adsorption sites cannot be larger for isoalkanes than for *n*-alkanes and the adsorption entropies of isoalkanes should be larger. It is rather improbable that branched and more bulky molecules have a higher mobility and retain more degrees of freedom in these narrow micropores. The data on adsorption entropies and enthalpies can be reconciliated assuming pore mouth adsorption. In the preferred adsorption modes, an *n*-alkyl group of the molecule penetrates into the micropore, while the bulky part including the branching is interacting with the external surface. Compared to the *n*-alkanes inside the pores, the isoalkanes in the pore mouths have a higher rotational and translational freedom, leading to higher preexponential factors.

Additional evidence for pore mouth adsorption of isoalkanes is provided with the adsorption isotherms (Figure 3). The adsorption capacity of ZSM-22 for isoalkanes is much reduced

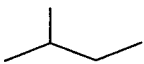
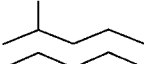
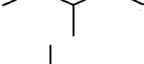
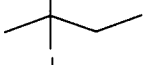
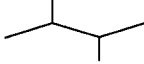
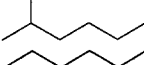
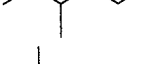
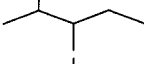
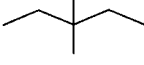
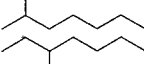
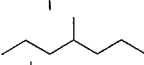
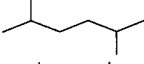
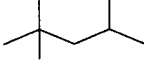
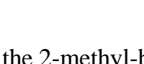
compared to the *n*-alkanes. This again indicates that mono-branched isomers do not occupy the entire micropore system of ZSM-22. 2-Methylhexane has an adsorption capacity of 40 $\mu\text{mol/g}$ at 233 °C. If only adsorption in the pore mouths is considered, the saturation capacity would be on the order of 0.34 $\mu\text{mol/g}$. A monolayer coverage of the total external surface would yield 500 μmol isopentane/g. In the Henry region, branched alkanes adsorb preferentially in the pore mouths. At higher partial pressures, the largest part of the molecules adsorb on the large external surface of ZSM-22.

The adsorption capacity of 2,3-dimethylbutane is very low. This molecule is very rigid, has very short *n*-alkyl chains (methyl groups only), and cannot be favorably adsorbed in pore mouths and, eventually, on the zeolite outer surface.

Beta, ZSM-5, and Mordenite Zeolites. On this family of zeolites, branched alkanes have lower preexponential factors than *n*-alkanes, pointing at a lower number of adsorption sites and/or higher losses of degrees of freedom in comparison with *n*-alkanes. In these zeolites, the adsorption of *n*- and isoalkanes occurs inside the channels. These zeolites exhibit peculiar adsorption behaviors that can be designated as manifestations of molecular shape selectivity.

On a nonpolar, nonporous adsorbent such as dimethylsilicone, 3-methyl-branched isomers adsorb stronger than 2-methyl-branched alkanes, in agreement with their relative volatility.¹¹ On all zeolites investigated except zeolite Y, the Henry constant for 2-methyl-branched alkanes is larger than for 3-methyl-

TABLE 10: Separation Factors between Linear and Branched Alkanes on ZSM-22, ZSM-5, Beta, and Mordenite at 573 K

| Temperature (°C) | | 573 K | | | |
|------------------------|---|--------|-------|------|-----------|
| | | ZSM-22 | ZSM-5 | Beta | Mordenite |
| 2-methylbutane |  | 4.1 | 1.5 | 1.6 | 1.5 |
| 2-methylpentane |  | 4.8 | 1.6 | 1.8 | 1.9 |
| 3-methylpentane |  | 5.9 | 1.8 | 2.2 | 2.7 |
| 2,2-dimethylbutane |  | 19.9 | 2.9 | 6.7 | 3.9 |
| 2,3-dimethylbutane |  | 10.8 | 3.1 | 3.3 | 3.5 |
| 2-methylhexane |  | 4.1 | 1.8 | 1.8 | 1.9 |
| 3-methylhexane |  | 5.3 | 1.9 | 2.5 | 3.6 |
| 2,3-dimethylpentane |  | 11.1 | 4.6 | 5.4 | 6.8 |
| 3,3-dimethylpentane |  | - | 2.8 | 8.1 | 8.5 |
| 2-methylheptane |  | 4.3 | 1.8 | 1.8 | 1.9 |
| 3-methylheptane |  | 5.9 | 2.2 | 2.5 | 4.0 |
| 4-methylheptane |  | 6.1 | 2.2 | 2.9 | 6.1 |
| 2,5-dimethylhexane |  | 14 | - | 3.2 | - |
| 2,2,4-trimethylpentane |  | 29 | > 30 | 18 | 13 |

branched alkanes (Figure 1). Generally, the 2-methyl-branched isomer has a higher adsorption enthalpy than the 3-methyl-branched isomer (Table 6). Preferential adsorption of the 2-methyl-branched alkanes on zeolite beta has been observed previously.^{5,6,8} It is concluded that in zeolites with pores that are narrower than in zeolite Y, molecular shape selective effects perturb the physisorption behavior of monomethyl-branched alkanes.

On ZSM-5, 2,2-dimethylbutane and 3,3-dimethylpentane have a larger Henry constant than 2,3-dimethylbutane and 2,3-dimethylpentane, respectively (Table 3). The molecule with quaternary carbon atom and kinetic diameter of 6.3 Å has larger adsorption equilibrium constants than the molecules with vicinal methyl side chains and a kinetic diameter of only 5.8 Å, which is a significant difference, certainly in comparison to the maximum crystallographic pore diameter of ZSM-5 (5.6 Å). A similar result with 2,2-dimethylbutane and 2,3-dimethylbutane was obtained earlier by Cavalcante and Ruthven.⁸ On zeolite beta and mordenite, 2,3-dimethylalkanes are adsorbed more strongly than 2,2-dimethylalkanes (Table 3); this is in contrast to ZSM-5. Another remarkable difference between beta, mordenite and ZSM-5 is that on mordenite and beta, Henry constants of monobranched alkanes decrease in the order K' -(2Me-branched) > K' -(3Me-branched) > K' -(4Me-branched), while on ZSM-5, 3- and 4-methylheptane have the same Henry constant.

Separation of Linear and Branched Alkanes. Except the Y type zeolites, the investigated zeolites show strongest adsorption of linear alkanes. The separation potential of these zeolites

for mixtures of linear and branched alkanes was evaluated based on separation factors, defined as (Table 10)

$$\alpha_{ij} = \frac{K'_i}{K'_j} \quad (12)$$

For C₅–C₈ alkanes, the largest separation factors are found on ZSM-22. On this adsorbent, the separation of linear and monobranched alkanes is considerably better than on the other zeolites. Among the C₈ alkanes, the separation factors for 2,5-dimethylhexane and 2,2,4-trimethylpentane on ZSM-5 and ZSM-22 are much larger than on the 12 MR zeolites.

The separation potential of ZSM-22 and its superiority to zeolite beta is confirmed in the chromatographic separation experiments with mixtures of alkanes in the C₅–C₈ range (Figures 4 and 5).

Conclusions

Henry constants, adsorption enthalpies, and van't Hoff preexponential factors of branched alkanes differ strongly from zeolite to zeolite. Minor differences in molecular shape and zeolite topology have a dramatic influence on the adsorption behavior.

On zeolite Y (12 MR), isoalkanes are adsorbed preferentially over linear alkanes. Zeolites beta (12 MR), mordenite (12 MR), ZSM-5 (10 MR), and ZSM-22 (10 MR) adsorb preferentially the *n*-alkanes. For the latter zeolites, Henry constants decrease in the order *n*-alkane > monomethyl-branched alkane >

dimethyl-branched alkane > trimethyl-branched alkane. Based on the values for the adsorption enthalpies and the van't Hoff preexponential factors, it is concluded that in the temperature range investigated (498–648 K) the C₅–C₈ isoalkanes have access to the intracrystalline micropore structures of zeolite Y, beta, mordenite, and ZSM-5. Under these conditions, mono- and multibranched C₅–C₈ alkanes have no access to the pores of ZSM-22 and are adsorbed initially in the pore mouths and at higher pressures on the external surfaces of the crystals.

Chromatographic separation experiments revealed that zeolites ZSM-22 and beta might be used to separate pentane, hexane, heptane, and octane isomers according to their branching degree.

Acknowledgment. This research received support from IWT (scholarship to J.D. and W.S.), the National Science Policy Office (IUAP-P4/11 Program on Supramolecular Catalysis), and the Flemish F.W.O. (Research Grant to G.B. and P.J. (G.B. 9.0231.951)).

References and Notes

- (1) Weisz, P. B. *Pure Appl. Chem.* **1980**, 52, 2091–2103.
- (2) Martens, J. A.; Souverijns, W.; Jacobs, P. A. In *Solid State Supramolecular Chemistry: Two and Three-Dimensional Inorganic Networks*; Alberti, G., et al., Eds.; Pergamon Press: New York, 1996; pp 621–646.
- (3) Chen, N. Y.; Garwood, W. E.; Dwyer, F. G. *Shape Selective Catalysis in Industrial Applications*; Marcel Dekker: New York, 1989.
- (4) Broughton, D. B. *Chem. Eng. Prog.* **1968**, 64 (8), 60–65.
- (5) Huddersman, K.; Klimczyk, M. *J. Chem. Soc., Faraday Trans.* **1996a**, 92 (1), 143–147.
- (6) Huddersman, K.; Klimczyk, M. *AIChE J.* **1996b**, 42 (2), 405–408.
- (7) Funke, H. H.; Kovalchick, M. G.; Falconer, J. L.; Noble, R. D. *Ind. Eng. Chem. Res.* **1996**, 35 (5), 1575–1582.
- (8) Cavalcante, C. L.; Ruthven, D. M. *Ind. Eng. Chem. Res.* **1995a**, 34, 177–184.
- (9) Cavalcante, C. L.; Ruthven, D. M. *Ind. Eng. Chem. Res.* **1995b**, 34, 185–191.
- (10) Choudhary, V. R.; Singh, A. P.; Kumar, R. *J. Catal.* **1991**, 129, 293–296.
- (11) Castello, G.; d'Amato, G. *J. Chromatogr.* **1975**, 107, 1–13.
- (12) Santilli, D. S.; Harris, T. V.; Zones, S. I. *Microporous Mater.* **1993**, 1, 329–341.
- (13) Martens, J. A.; Parton, R.; Uytterhoeven, L.; Jacobs, P. A.; Froment, G. F. *Appl. Catal.* **1991**, 76, 95.
- (14) Martens, J. A.; Souverijns, W.; Verrelst, W.; Parton, R.; Froment, G. F.; Jacobs, P. A. *Angew. Chem., Int. Ed. Engl.* **1995**, 34, 2528–2530.
- (15) Denayer, J. F. M.; Baron, G. V.; Martens, J. A.; Jacobs, P. A. In press.
- (16) Meier, W. M.; Olson, D. H. *Atlas of Zeolite Structure Types*; Butterworth-Heinemann: London, 1992.
- (17) Ernst, S.; Weitkamp, J.; Martens, J. A.; Jacobs, P. A. *Appl. Catal.* **1989**, 48, 137–148.
- (18) Caullet, Ph.; Guth, J.-L.; Faust, A. C.; Raatz, F.; Joly, J. F.; Deves, J. M. *EP 419, 334* **1991**, example 5.
- (19) Ruthven, D. M. *Principles of Adsorption and Adsorption Processes*; John Wiley and Sons: Canada, 1984.
- (20) Hufton, J. R.; Danner, R. P. *AIChE J.* **1993**, 39 (6), 954–961.
- (21) Denayer, J. F. M.; Baron, G. V. *Adsorption* **1997**, 3, 261–265.
- (22) Highcock, R. M.; Smith, G. W.; Wood, D. *Acta Crystallogr.* **1985**, C41, 1391.
- (23) Pickett, S. D.; Nowak, A. K.; Thomas, J. M.; Cheetham, A. K. *Zeolites* **1989**, 9, 123.
- (24) Jänchen, J.; Stach, H. *Adsorpt. Sci. Technol.* **1986**, 3, 3–10.